Human neural stem cell secretome relieves endoplasmic reticulum stress-induced apoptosis and improves neuronal functions after traumatic brain injury in a rat model

Yating Ling
Jiangsu University
Murugan Ramalingam
Dankook University
Xiaorui Lv
Jiangsu University
Dongdong Niu
Jiangsu University
Yu Zeng
Jiangsu University
Yun Qiu
Jiangsu University
Yu Si
Jiangsu University
Tao Guo
Jiangsu University
Yinying Ni
Jiangsu University
jingwen Zhang
Jiangsu University
Ziyu Wang
Health BioMed Co., Ltd. Ningbo
Jiabo Hu
hu@ujs.edu.cn
Jiangsu University

Research Article

Keywords: Traumatic brain injury, Endoplasmic reticulum stress, Neural stem cells, Secretome, Calumenin

Posted Date: October 28th, 2023

DOI: https://doi.org/10.21203/rs.3.rs-3476710/v1

Additional Declarations: No competing interests reported.

Version of Record: A version of this preprint was published at Journal of Molecular Histology on April 12th, 2024. See the published version at https://doi.org/10.1007/s10735-024-10192-7.

Abstract

Neural stem cell secretome (NSC-S) plays an important role in neuroprotection and recovery. Studies have shown that endoplasmic reticulum stress (ER stress) is involved in the progression of traumatic brain injury (TBI) and is a crucial cause of secondary damage and neuronal death after brain injury. Whether NSC-S is engaged in ER stress and ER stress-mediated neuronal apoptosis post-TBI has not been investigated. In the study, the Feeney SD male rat model was established. The results indicated that NSC-S treatment could significantly improve the behavior of TBI rats and reduce the area of brain contusion in rats. In addition, NSC-S relieved ER stress in TBI rats and was observed by transmission electron microscopy and western blot. The specific mechanism was further elucidated that restoration was achieved by alleviating the PERK-eIF2α pathway and thus protecting neurons from apoptosis. Notably, the discovery of calumenin (CALU) in NSC-S by liquid chromatography-tandem mass spectrometry (LC-MS/MS/MS) may be related to the protective effect of NSC-S on ER stress in neurons. Also, the mechanism by which it functions may be related to ubiquitination. In summary, NSC-S improved prognosis and ER stress in TBI rats and might be a promising treatment for relieving TBI.

Introduction

Traumatic brain injury (TBI) is a sudden injury caused by an external force such as a fall or road traffic accident that causes damage to the brain, which is also considered one of the leading causes of death in adolescents and children throughout the world(Sun et al. 2021). It is estimated that 69 million people suffer from TBI for various reasons every year(Chen et al. 2020a) and considered a serious health problem and medical burden worldwide. The pathophysiology of TBI includes primary destruction of brain tissue and subsequent secondary response(Chen et al. 2020b; Prins et al. 2013; Li et al. 2019).

Primary injury tends to have a short incubation period(Capizzi et al. 2020), and it is easy to miss the optimal rescue time. In contrast, persistent secondary injury of the brain after hours or days has attracted the focus of researchers. The secondary injury involves complex pathological mechanisms(Deng et al. 2021). Also, it caused secondary neuronal deaths, which are the leading causes of post-TBI(Nakka et al. 2016; Chen et al. 2020b). For decades, the main therapeutic approach has been used to treat damaged tissue with interventions to reduce lesion size and decrease neuronal death. Over the past 30 years, more than 30 clinical trials and multiple drug therapies have been initiated for the potential treatment of TBI, and almost all phase II/III TBI clinical trials have failed (Loane and Faden 2010; Xiong et al. 2015; Khellaf et al. 2019); therefore, an urgent need to elucidate the specific mechanisms of TBI and investigate the effective therapeutic strategies to reduce TBI-induced neuronal death.

Endoplasmic reticulum stress (ER stress) has recently paid remarkably increasing attention to the pathogenesis of various neurodegenerative diseases, including cerebral ischemia, TBI, Alzheimer's, and Parkinson's disease(Kim et al. 2008; Wang et al. 2019; Kaufman 2002; Larner et al. 2006). Ischemia and hypoxia destroy calcium homeostasis or protein folding abnormalities, which may cause ER stress, and activate the unfolded protein response, also continuous stress can lead to cell death(Nakka et al. 2016).

Clinical studies have shown that brain tissue in TBI patients is highly expressed ER stress-related indicators(Lucke-Wold et al. 2017; Wu et al. 2022). Furthermore, inhibition of ER stress attenuates TBI-related pathological apoptosis and improves TBI-induced neurological dysfunction and rat behaviors(Begum et al. 2014; Sun et al. 2020; Wu et al. 2019; Xiong et al. 2020; Gao et al. 2022). Therefore, it is expected to treat TBI by relieving neuronal ER stress.

Recently, neural stem cell (NSCs) therapy has had a remarkable interest. NSCs can secrete a variety of nutrient factors, such as BDNF, NT3, GDNF, etc.(Ratajczak et al. 2012; Lu et al. 2003; Borhani-Haghighi and Mohamadi 2021). Also, it can secrete a multitude of unknown nutrients, which in turn protect the damaged cells(Yang et al. 2018). The secretome is a group of molecular and biological factors secreted by these cells into the extracellular space (Daneshmandi et al. 2020; Ni et al. 2022; Zhou et al. 2022).

Preliminary studies conducted in the laboratory have found that the neural stem cell secretome (NSC-S) has a certain effect on inhibiting inflammation and resisting oxidative stress(Chen et al. 2020a; Tang et al. 2021). Also, NSC-S improves Aβ25-35-induced SH-SY5Y cell damage by protecting mitochondrial function(Jia et al. 2021), and easing rotenone-induced toxicity in SH-SY5Y cells(Ramalingam et al. 2021). In addition, NSC-S has a distinct therapeutic and neuroprotective effect on TBI rats(Salikhova et al. 2021; Tsai et al. 2014). However, ER stress causes oxidative stress, inflammation, mitochondrial damage, etc. Therefore, the restoration of NSC-S on TBI and the substances that play a role in NSC-S will be evaluated in this study. Also, Further studies need to explore a specific mechanism of how NSC-S plays a protective role in restoring neuronal functions.

Materials and methods

NSC-S preparation

According to previous studies(Chen et al. 2020c), NSCs were derived from the differentiation of human embryonic stem cells (hESCs), which were purchased from the Cell Bank of the Chinese Academy of Sciences. Briefly, NSCs were cultured in Dulbecco's modified Eagle's medium Nutrient Mixture F-12 (DMEM/F-12) (Gibco, USA) supplemented with 1% penicillin-streptomycin, 20 ng/mL basic fibroblast growth factor (bFGF) and 20 ng/mL epidermal growth factor (EGF) (PeproTech). Serum-free DMEM (Gibco, USA) was added when the NSCs confluence reached 90%. After 12 h, the NSC-S were collected and centrifuged at 2000 rpm for 20 min to ensure that the NSC-S didn’t contain intracellular contents.

For in *vivo* experiments, NSC-S was concentrated 10-fold by the freeze dryer (Labconco FreeZone, England) and stored at − 80°C. Meanwhile, concentrated 10-fold DMEM was prepared by treating DMEM in the same way and served as a control (Tang et al. 2021; Ni et al. 2022; Zhou et al. 2022).

TBI model

SD male rats, weighing 260–280 g were purchased from the animal experiment center of Jiangsu University (Zhenjiang, China). Generally, male rats are stronger than females. Also, other factors (food,

living environment, hormones, etc.) can easily interfere with the experimental results. The experimental results of male rats are easy to achieve the expected results. All animal experiments were approved by the institutional animal care and use committee of Jiangsu University (Permit Number: SCXK 2018-0012).

All rats were randomly assigned into a sham group, TBI group, and TBI + NSC-S group. The TBI model was developed with slight modifications from the Feeney free-fall model(Wu et al. 2021). TBI was induced in the anesthetized (50 mg/kg pentobarbital; intraperitoneally) rats. Briefly, a midline incision was made over the skull, and a 5-mm craniotomy was drilled through the skull 2.5 mm caudal to the left coronal suture and 2.5 mm from the midline without disturbing the dura. TBI was induced using a weight-drop hitting device with a 4.5-mm-diameter cylinder bar weighing 50 g from a height of 15 cm (Chen et al. 2018). After surgery, the scalp was sutured and antibiotics were applied to prevent infection. All procedures were the same for each group except in the sham group, in which no weight was dropped.

After 24 h, the TBI + NSC-S group was injected with 10 μL of 10×NSC-S. The fontanelle coordinates are (0,0,0,) and the injection sites were (0, -2.5, -3) and (5, -2.5, -3), with 5 μL of each site injected. The velocity of injection was 0.5 μL/min(Pang et al. 2017). The scalp was finally sutured and the suture was coated with antibiotics applied to the suture to prevent infection.

Behavior evaluation

All behavioral tests were done by researchers in a sterilized environment with controlled temperature, humidity, and noise. All equipment was sterilized for use before each test.

Modified neurological severity score (mNSS)

mNSS were used to assess neurological deficits. Rats were examined for motor (muscle status and abnormal movements), sensory (visual, tactile, and balance), and reflexes. Then the score when tasks were not completed or the corresponding reflexes were lost. mNSS tests were graded on a scale of 0–18, with a total score of 18 indicating severe neurological deficits(Xu et al. 2021). The performance of the rats was evaluated on days 0, 1, 3, 7, and 14 d after surgery.

Foot fault test

The foot fault test is sensitive to deficits in descending motor control(Mao et al. 2021). Rats with impaired motor function were more sensitive to foot fault tests. Place them in a grid measuring 100 cm × 100 cm and mesh size 3 cm × 3 cm, 1m above the floor. The rats were observed in the grid, and the number of forelimbs stepping in 50 steps was counted three times each.

Beam walking test

The balance beam device is a beam with dimensions of 3 cm × 3 cm × 100 cm. Three days before the experiment, the rats were placed at one end of the balance beam and given light and noise stimulation; the stimulation was stopped after they entered the black box from one end and the rats were kept in the black box for more than 30 seconds. The rats were trained 3 times a day till the modeling. Balance beam

experiments were performed on days 0, 1, 3, 7, and 14 after surgery, and the performance of the rats on the balance beam was recorded. The specific scoring criteria are shown in Table 1(Liu et al. 1994).

Table 1
Beam walking test score

Score	*Behavior*
1	able to maintain balance with all four paws on the surface of the balance beam
2	holding the paws on the side of the balance beam/shaking
3	having one and two limbs fall
4	having three limbs fall
5	trying to balance but slipping
6	failing to try to balance, hanging on the balance beam, and falling
7	falling directly without trying to balance

Hang wires test

The suspension bar apparatus consisted of two 100 cm high vertical support bars and a wooden stick with a diameter of 3 cm and a length of 100 cm(Mao et al. 2021). The whole device was placed flat; the rats were placed in the suspension position of the wooden stick and observed each trial for 20 seconds, and repeated 3 times. The behavior of the rat hanging on the wooden stick was recorded and scored according to the following criteria, as shown in Table 2.

Table 2
Hang wires test

Score	*Behavior*
0	directly off
1	hanging on the stick with two forelimbs
2	hanging on the stick with two forelimbs and trying to climb up the stick
3	hanging on the stick with both forelimbs and one or two hind limbs
4	all four paws on the stick and the tail wrapped around the stick
5	escaping to either side of the support bar

Open-field test

The open-field test is widely used to assess the general exploratory activity of rodents as they instinctively try to explore open areas. Rats were confined to a 100 cm × 100 cm box, the entire area was kept quiet, the room was dimly lit, and researchers left the room after the device worked properly. Infrared

light recordings track the rats' movements over 30 min and assess their preference for the open area of the device to estimate TBI-induced anxiety behavior in rats(Tang et al. 2021).

Elevated maze test

The elevated maze experiment is a commonly used behavioral paradigm for assessing anxious ambivalence in rodents due to intense approach-avoidance conflict(Moritz et al. 2014). Post-injury day 3, the animals were placed in the center of the maze, where the open and closed arms were crossed. They were allowed to explore freely for 5 min, during each time the movement monitoring software assessed the animals' movements. The number and duration of entries into the open and closed arms and the ratio were calculated.

HE staining / Nissl staining

Rat brains were removed, and soaked with 4% paraformaldehyde for 24 h. The tissue was embedded in paraffin and cut into sections of 3 μm thickness. According to the reagent's instructions, the brain tissues were dewaxed twice with xylene, treated with gradient ethanol dehydration, stained with hematoxylin-eosin staining (HE) or Nissl 's reagent (Solarbio, Beijing), and sealed with neutral resin after clear treatment with xylene. The brain sections were scanned with a Pathological slice sweeper (3DHistech, Hungary).

Co-culture of PC12 cells with NSCs

PC12 cell culture

PC12 cells were purchased from the cell bank of the Chinese Academy of Sciences and were a highly differentiated cell line. Cells were cultured in Dulbecco's modified Eagle's medium (DMEM) (Gibco, USA) with 3% heat-inactivated bovine serum (NBS; Gibco, USA) and 1% penicillin-streptomycin. Cells were grown in 5% CO_2 at 37℃ in a humidified incubator.

Transwell co-culture system

PC12 cells and NSCs were co-cultured in a six-well plate transwell system (Thermo Fisher, USA). Two types of cells co-cultured in a 1:1 ratio, with NSCs seeded in the upper chamber and PC12 cells in the lower chamber. The two cells were cultured with their respective culture medium for 24 h, and PC12 cells were treated differently and then co-cultured with NSCs. The co-culture system used a PC12 cell culture medium.

Cell viability

Cell viability was determined by MTT (Macklin, China). PC12 cells were grown in 96-well plates at a density of 5×10^4/well, and incubated for 24 h, followed by changing the medium with MTT mixture (MTT: DMEM = 1:9) and continuing the incubation for 4 h. MTT mixture was removed and added 150 μL DMSO solution to each well. Finally, an enzyme marker (BioTek, USA) was used at 450 nm and the optical density (OD) of each well was measured.

Cytoplasmic calcium ion levels

Calcium ion alterations in cells were monitored using flu-3/AM (Beyotime, China) by flow cytometry or fluorescence microscopy as a Ca^{2+} fluorescent indicator(Wang et al. 2021). Cells were incubated at 37°C for 30 min, providing 5% CO_2 to ensure complete esterification of the probe. For flow cytometry observation, the collected cells were resuspended in 200μL PBS (Beckman Coulter, USA) within 1 h; For immunofluorescence microscopy, the probe was removed, then collected cells were washed 3 times with PBS for 5 min each, and fluorescence microscope (OLYMPUS, Japan) was used for observation.

Ca^{2+}-ATPase activity

The Ca^{2+}-ATPase activity (Nanjing Jiancheng, China) was determined as previously described. Briefly, centrifugation of the cells in a 6-well plate to extract the precipitate(Chang et al. 2016; Wang et al. 2021), resuspension in saline, then sonication of the cells (300 W, 5 s at each time, 5 s interval, 4–5 cycles). Finally, the supernatant was added to a 96-well plate for colorimetry at 636 nm (BioTek, USA).

Reactive oxygen species (ROS)

The production of intracellular reactive oxygen species was measured using the fluorescent probe DCFH-DA (Beyotime, China. Cells in a 6-well plate were incubated with 10 μM DCFH-DA in a dark room for 1 h. Then collected into EP tubes, washed twice with PBS, and resuspended for detection using flow cytometry (Beckman Coulter, USA).

ER Tracker staining

ER Tracker (Beyotime, China) is commonly used as an ideal fluorescent probe for endoplasmic reticulum tracking(Wan et al. 2021; Lima et al. 2019; Xing et al. 2019). PC12 cells were washed once with serum-free DMEM, and pre-warmed ER Tracker (1:1000) was added and incubated for 20 min at 37°C. The stain was removed, fixed in 4% paraformaldehyde for 2 min, then restained in DAPI, and washed with PBS to remove non-specific staining. Finally, observed under a microscope (OLYMPUS, Japan).

Apoptosis

Cells in 6-well plates were digested with trypsin without DTA and washed three times with cold PBS (800 rpm for 5 min). Cells were then resuspended in 400 μL of binding buffer with FITC-Membrane Linker V (5 μL) and PI (5 μL) and incubated for 15 min at 4°C in the dark. Apoptosis analysis was performed using flow cytometry (Beckman Coulter, USA) within 1 h.

Transmission electron microscopy (TEM)

Immediately after cell or tissue collection, brain tissue samples were fixed in 2.5% glutaraldehyde overnight at 4°C, post-fixed with 1% osmium tetroxide for another 1 h, dehydrated in a series of graded ethanol solutions for 30 min, then gradually embedded in epoxy resin. Ultrathin sections (60–90 nm) were cut with a diamond knife, double-stained with uranyl acetate and lead citrate, and then examined with a Hitachi-h7650 electron microscope, and representative images were analyzed.

Immunofluorescence

For the in *vivo* experiments, coronal sections were prepared. For the in vitro experiments, cell cultures were discarded from the original culture, and washed 2 times with PBS. Then both were fixed with 4% paraformaldehyde for 30 min, permeabilized with 0.1% TritonX-100 for 30 min, and blocked with 5% BSA for 1 h. Then, incubated with a specific primary antibody for 4℃ overnight (Table 3). The next day, the cells were washed with PBS and incubated with FITC-coupled secondary antibody for 1 h. Finally, DAPI was used to restain. The nuclei were washed with PBS to reduce non-specific staining and observed with fluorescence microscopy (OLYMPUS, Japan).

Western blot

Rats were deeply anesthetized with pentobarbital (50 mg/kg, intraperitoneally) and decapitated. After the removal of the brain, the right cortical tissue was dissected on a cooled ice plate and the brain tissue around the site of injury was selected for western blot. Cell cultures were discarded from the original culture, and washed 2 times with PBS. Tissue and cells were treated with ice-cold lysis buffer (100 μL RIPA, and 1 μL protease inhibitor) (Beyotime, China). Total protein content was determined using a nucleic acid protein assay (Eppendorf, Germany). Protein samples were loaded (100 μg total protein/lane) and electrophoresed in 12% sodium dodecyl sulfate-polyacrylamide gel electrophoresis (SDS-PAGE) gels for 2 h and transferred to polyvinylidene difluoride (PVDF) membranes (Sigma, USA). The membranes are then blocked with 5% skim milk for 2 h at room temperature and incubated overnight at 4℃ with primary antibody (Table 3). The next day membranes were washed three times with Tris-buffered saline with Tween 20 (TBST) (Biosharp, China) and incubated with the fluorescent secondary antibody (1:5000 dilution) for 1 h. The protein signal was detected using an ECL substrate (Vazym, China), and the optical intensity of the protein bands was quantified using Lane1D.

Table 3
Complete antibody list for all immunofluorescence and Western blot

Antibody	Immunogen comment	Manufacturer, Catalog, and RRID	concentration
β-actin	Human β synthetic peptide immunity of residues near the amino terminus of actin	CST, Cat# 4970, Rabbit mAb, AB_2223172	WB 1:1000
GRP78	Synthetic peptide	Abcam, Cat# ab108615, Rabbit pAb, AB_10890641	WB 1:1000
PERK	Synthesis of PERK peptides	Wanlei, Cat# WL03378, Rabbit mAb	WB 1:1000
P-PERK	Synthesis of P-PERK (T982) peptide	Wanlei, Cat# WL05295, Rabbit mAb	WB 1:1000
eIF-2α	Synthesis of eIF2α peptides	Wanlei, Cat# WL01909, Rabbit mAb	WB 1:1000
P-eIF-2α	A synthesized peptide derived from human Phospho-EIF2S1 (S51)	Boster, Cat# BM3942, Rabbit mAb	WB 1:500
ATF-4	A synthesized peptide derived from human ATF4	Boster, Cat# BM5179, Rabbit mAb	WB 1:1000
CHOP	Synthetic peptide immunity of human CHOP sequences	CST, Cat# 2895, Mouse mAb, AB_2089254	WB 1:1000 IF 1:200
Ubiquitin	Denatured glutaraldehyde cross-linked ubiquitin IgG complex	Biolegend, Cat# 646301, Mouse mAb, AB_1659270	WB 1:1000
SERCA	Synthesis of ATP2A1/SERCA1 polypeptides	Wanlei, Cat# WL02684, Rabbit mAb	WB 1:1000
MAP2	MAP2 fusion protein Ag11349	Proteintech, Cat# 67015-1-Ig, Mouse mAb, AB_2882331	IF 1:200
NF	E.coli-derived human NEFL/NF-L recombinant protein	Boster, Cat# A02482-1, Rabbit pAb	IF 1:200

qRT-PCR

Total RNA was extracted using RNA-easy™ isolation reagent (Vazyme, China) according to the manufacturer's instructions. Total RNA concentration and purity were determined with a nucleic acid protein assay (Eppendorf, Germany). A260/A280 for RNA was 1.8-2.0, and the concentration was about 300 mg/ml. The cDNA was prepared by using a Quantscript RT Kit (Vazyme, China). The cDNA was mixed with the SuperReal PreMix Plus kit (SYBR Green, Vazyme, China) for qRT-PCR. The results were analyzed by the $2^{-\Delta\Delta Ct}$ method. The primer pairs sequences for gene amplification are listed in Table 4:

Table 4
Primer sequences used for qRT-PCR

Primer name	Sequence (5'–3')	Amplicon length(bp)
β-actin	F-GCTGTGCTATGTTGCCCTAGACTTC	122
	R-GGAACCGCTCATTGCCGATAGTG	
Derlin1	F-GCCGTTCACTGCCACCTTTTATTTC	104
	R-CTGCCTCAAGCCGTGTAGAATACTG	
Derlin2	F-TGGAGCCGACGGAACCCATATG	84
	R-GATGAGCACCCAGGGCAGAAAG	
Derlin3	F-CATGGGCTTCTCGCTGCTTCTG	107
	R-CAGGCTGGTTGGGAAAGACATCTTC	
EDEM1	F-CCTGGTTGATGCCTTGGATACACTC	122
	R-CCTCAAAGACTTGGACGGTGGAATC	
HRD1	F-GTTGGCTGAAGACCGTGTGGAC	95
	R-TGCCCAGGAGGAACATAAGAGAGAC	
HERP1	F-AAGCCAGAAGCCAGCACAAAGAG	111
	R-GACTTCCCTTTCCCGAAGCCATC	
SERCA	F-CTGCTCACTGAACGAGTTCTCCATC	113
	R-CAAGTTCCACCAGCCCGTCATAC	

Liquid Chromatography-Tandem Mass Spectrometry (LC-MS/MS) for NSC-S

After the successful collection of NSC-S, NSC-S was analyzed by LC-MS/MS. The NSC-S was vacuum freeze-dried, enzymatically lyzyed, and peptide desalted, and the final collected samples were analyzed using nano-UPLC (EASY-nLC1200) with the Q Exactive HFX Orbitrap instrument (Thermo Fisher Scientific) with a nano-electrospray ion source. Finally, the obtained results were analyzed by bioinformatics technology such as GO, KEGG, PPI, etc.

Statistical analysis

All data are represented as standard deviations (SD). All data were tested for Shapiro-Wilk normality ($P > 0.5$). The t-test was used to compare the two groups. For assessing the differences among three or more groups, if all the variables meet homogeneity of variance, one-way analysis of variance (ANOVA) was used to compare three or more groups, and Tukey honest test was used for the post-hoc test. The Brown-Forsythe test was used to compare three or more groups, and the Games-Howell test was used for the

post-hoc test. Two-way ANOVA analysis was used for bivariate data. Each experiment was carried out independently at least three times. $P < 0.05$ is considered statistically significant.

Results

NSC-S improves behavior disorders in the TBI rat model

The experimental protocol for the sham group, TBI group, and TBI + NSC-S group was described in Fig. 1a. Firstly, the TBI model was established using the classical Fenney model (Fig. 1b), and then a series of tests were done. mNSS was performed on rats on days 0 to 14 post-TBI to evaluate the effects of NSC-S on the neurological function of TBI rats. As shown in Fig. 2c, the neurological function began to recover between the 3rd and 14th days post-TBI and treatment with NSC-S decreased mNSS between the 3rd and 7th days post-TBI. Beam walking tests, forelimb stepping experiments, and hang wire tests were carried out to assess the sensorimotor function of TBI rats. Treatment with NSC-S improved motor function in the corresponding group compared with the sham group during the 1st, 3rd, and 7th days post-TBI (Fig. 1d-g). In addition, TBI rats treated with NSC-S showed longer movement distances, faster movement speed, and more exploration of the test apparatus (Fig. 1h-j).

NSC-S relieves neuronal injury in TBI rat model

As seen in Fig. 2a, the brain tissues taken out showed that NSC-S partially recovered the brain-size tissue damaged after TBI. Further confirmation by the HE staining results (Fig. 2b-c). Nissl staining is commonly used to visualize the internal structure of neurons and the neuron damage. TBI-induced neuron damage in the cortex was shown with Nissl staining (Fig. 2d). In the cortex area, the number of neurons with irregular cell bodies, shrinkage, and hyperchromatic nuclei increased in the TBI group. On the other hand, NSC-S treatment saved neurons from these changes.

NSC-S restores neuronal ER stress in the TBI rat model

Transmission electron microscopy (TEM) was used to observe the ER of rat brain tissue. In the sham group, the ER presented a typical luminal structure and was neatly arranged. However, partial fragmentation of the ER was observed in the TBI group. After the brain stereotaxic injection of NSC-S, its ER reverted to its original luminal structure (Fig. 3a). Consistent with this, NSC-S reduced the upregulation of ER stress marker protein GRP78 after TBI. And the ER stress pathway proteins PERK, eIF-2 , ATF-4, and CHOP were also significantly reduced after NSC-S treatment (Fig. 3b-c). CHOP is a key molecule linking ER stress to apoptosis cell death. The expression of this pro-apoptotic protein was checked in the ipsilateral cortex 3 days after TBI. The administration of NSC-S after TBI significantly reduced the expression of the pro-apoptotic protein CHOP (Fig. 3d).

Co-culture with NSCs mitigates TG-induced PC12 cell damage

In *vitro*, the specific mechanism that NSC-S plays a protective role in neuronal ER stress continued to be explored in the study. Thapsigargin (TG) as the classic model drug for ER stress was chosen. First of all, changes in PC12 cell viability after TG induction in a dose-dependent manner were investigated, and the concentration of TG was determined when the cell viability decreased to 50% (0.2 μM) (Fig. 4a). After TG treatment, the morphology of PC12 cells became smaller and shrunken, and the number decreased. Meanwhile, the morphology and number of cells were restored after co-culture with NSCs, and cell viability was restored to approximately 74.8% (Fig. 4b-c). In addition, PC12 cells showed shorter axon length and increased cytotoxic ROS levels after TG treatment, while after co-culture with NSCs, the axon length of PC12 cells increased and cytotoxicity decreased (Fig. 4d-f).

Co-culture with NSCs relieves TG-induced PC12 ER stress

As a classic ER stress inducer, TG can disrupt ER calcium ion disorders and activate cells to develop ER stress. As shown in Fig. 5a-c, indicators related to calcium ion levels were detected. The Ca-ATPase levels of PC12 cells were significantly enhanced in the co-culture group. In addition, the flow cytometry results showed that cytoplasmic calcium homeostasis was restored. To further confirm the effect of co-culture treatment on ER stress in PC12 cells, TEM was then used to observe the morphology of the ER. The results showed that exposure to TG induced marked ultrastructure abnormality in PC12 cells. In respect of ER, swelling, and dilatation appearing as a large number of vacuoles was the main change in the TG group. However, in the co-culture group, these abnormal morphological changes in the ER were barely detected (Fig. 5d). Subsequently, the ER was localized by the ER Tracker probe. The fluorescence intensity of the probe decreased after injury, and it was recovered after co-culture with NSCs (Fig. 5e). Additionally, TG exposure changed the expression of several typical ER stress marker proteins in PC12 cells. As shown in Fig. 5f-g, the marker protein GRP78 was associated with ER stress, and the ER stress pathway proteins PERK, eIF-2 , ATF-4, and CHOP were detected, and found that TG significantly increased the expression of ER stress-related proteins. However, these indicators were significantly reduced after co-culture.

Co-culture with NSCs inhibits TG-induced ER stress through the PERK pathway

The protein interaction diagram showed that the TG-induced ER stress mechanism was closely related to the PERK pathway (Fig. 6a). Interestingly, NSC-S reduced the protein level of the PERK pathway. However, PERK activator CCT020312 administration restored the inhibition effect of NSC-S on PERK pathway protein (Fig. 6b-c), and flow cytometry results also indicated that CCT020312 significantly blocked the decrease in apoptosis induced by NSC-S (Fig. 6d).

Bioinformatics analysis of LC-MS/MS result on NSC-S

Kyoto Encyclopedia of Genes and Genomes (KEGG) analysis of the top 20 enriched pathways identified a pathway related to ER protein processing and speculated to be associated with ER stress. Calumenin (CALU) was found among the proteins involved in this pathway, which could regulate ER calcium

homeostasis and was associated with calcium pump activity (Fig. 7a). Gene Ontology (GO) analysis revealed that CALU was involved in most biological processes and could be secreted into the extracellular (Fig. 7b). The interacting proteins of CALU were predicted through the STRING website, and CALU was found to be closely associated with ER stress-related proteins (Fig. 7c). The relative concentration of CALU in NSC-S was about 90 times more than that of DMEM (Table 5).

Table 5
Different expressions of CALU in NSC-S (MEAN A) and DMEM (MEAN C)

GeneName	Accession	Description	MEAN A	MEAN C	FOLD CHANGE
CALU	O43852	Calumenin	408131.0684	4452.394669	91.66551905

The CALU recombinant protein relieves ER stress in TG-induced PC12 cells

After adding CALU recombinant protein, the morphological changes of the cells were first observed. CALU ameliorated TG-induced morphological damage in PC12 cells, such as cell shrinkage and short axonal mutations (Fig. 8a). TG prevented calcium ions from entering the ER, leading to an increase in calcium ions in the cytoplasm; the addition of CALU maintained calcium ion homeostasis (Fig. 8b-c). The results of the ER-labeled ER tracker and calcium probe Fluo-3co-staining showed that TG increased the fluorescence intensity of Fluo-3 in PC12 cells, while the fluorescence intensity of the ER decreased; the addition of CALU reversed this action (Fig. 8d). Notably, western blot showed that CALU also reduced the levels of ER stress-related proteins. Flow cytometry analysis showed that the percentage of apoptotic cells decreased from 15.85 to 7.96% after CALU recombinant protein addition (Fig. 8e-g).

The CALU recombinant protein exerts protective effects by reducing cellular ubiquitination levels

After the addition of CALU recombinant protein, the activity of (Sarcoplasmic Endoplasmic Reticulum Calcium ATPase) SERCA increased by 3.12 times, and the protein expression level of SERCA was also significantly restored (Fig. 9a-c). In contrast, *SERCA*'s gene expression levels were the opposite of protein level results (Fig. 9d). It is speculated that it may be related to SERCA ubiquitination, as shown in Fig. 9e, after the addition of the ubiquitination inhibitor MG132, SERCA levels are restored. Intracellular ubiquitination levels were measured and found that CALU can reduce TG-induced elevation of ubiquitination levels. Ubiquitination inhibitors MG132 make suppression of ubiquitination levels (Fig. 9f). Protein interaction mapping analysis showed that CALU was associated with ubiquitination-related genes such as *Derlin, EDEM1, HERP1, and HRD1* (Fig. 9g). CALU can restore the expression of ubiquitination-related genes after TG induction (Fig. 9h).

Discussion

TBI, as one of the leading causes of death and disability worldwide, is a risk factor for dementia and stroke in later life(Jamjoom et al. 2021). However, the conventional treatment of TBI has adverse reactions to a greater or lesser extent, so stem cell therapy came into being.

Stem cells play an important role in nerve recovery, functional restoration, and tissue reconstruction(Zibara et al. 2019). Neural stem cell-based nerve therapies have neuroprotective abilities, which have been widely used in many disease models(Yu et al. 2013), particularly in brain diseases, such as Parkinson's, neuroinflammation, etc. Although NSCs transplantation positively affects central nervous system injury. However, these cells are difficult to survive at the site of injury, resulting in a weakened efficacy. Unlike NSCs transplantation, NSC-S contains a large number of active factors(Huang et al. 2018; Hwang et al. 2013), which can promote neuronal growth, and axon elongation, and solve the problem of immune rejection between co-receptors by collecting NSC-S instead of NSCs transplantation. Besides, NSC-S is well-sourced and can be produced in large quantities (Tang et al. 2021; Ni et al. 2022; Zhou et al. 2022). Thus NSC-S is considered an effective tool for cell-based therapy.

In this study, the effects of NSC-S on behavioral and neuronal ER stress in TBI rats were investigated in vivo. The classic Fenney TBI model was used, and a series of behavioral tests were performed on rats from day 0 to 14 after modeling. The results showed that the behavior of rats in the NSC-S group was significantly improved, especially in the beam walking experiment, and the brain stereotaxic injection of NSC-S caused the rats paralyzed in the beam walking experiment to move slowly. Also, TBI can significantly cause ER stress, which was confirmed by both TEM and western blot. The ER stress marker protein GRP78 and the ER stress pathway-related proteins PERK, eIF-2α, ATF4, and CHOP were all reduced after NSC-S. There is growing evidence that TBI is strongly associated with ER stress and may be a major cause of neuronal death after TBI. In addition, NSC-S reduced the area of brain contusion and neuronal death which was observed by HE and Nissl stain.

Although NSC-S plays an important role in TBI, the discovery of the specific mechanisms needs to be investigated. In vitro, TG is now considered to be one of the classic drugs for inducing ER stress(Abdullahi et al. 2017), which can target Ca-ATPase in the ER(Verfaillie et al. 2012). Calcium ions cannot enter the ER, which in turn leads to the depletion of ER calcium ions and then ER stress. Hence, TG-induced PC12 injury is considered as a classic in vitro model of neuronal ER stress. In addition, in vitro co-culture with NSCs was much better than NSC-S, which more realistically mimics the in vivo microenvironment.

It was found that co-culture with NSCs significantly restored the number and morphology of cells in the TG group and lengthened axons. Next, calcium-related indices were examined. Consistent with the expected results, co-culture with NSCs restored calcium homeostasis in PC12 cells. PERK is a protein kinase-like endoplasmic reticulate belonging to the transmembrane ER-resident protein(Bertolotti et al. 2000; Abdullahi et al. 2017). Its main function is to sense stress-related information transmitted by the ER(Verfaillie et al. 2012). When sustained ER stress occurred, PERK would dissociate itself from the chaperone protein and phosphorylation. It activated downstream pathways and eventually led to

neuronal apoptosis(Kumar et al. 2001; Begum et al. 2014). In the present study, co-culture with NSCs can achieve neuronal protection by inhibiting the PERK-eIF2 pathway to alleviate neuronal ER stress. However, CCT020312, a PERK activator, counteracted the protective effect exerted by co-culture with NSCs and increased ER stress in the cells after the addition of CCT020312 pretreatment. The level of apoptosis of the cells increased from 22.17–53.14% after the addition of CCT020312, indicating that NSC-S did exert a protective effect in a PERK-dependent manner.

To explore specific substances in NSC-S that play a specific regulatory role. Proteomics in NSC-S was identified by LC-MS/MS and bioinformatics was analyzed. KEGG analysis showed that one of the top 20 pathways in terms of enrichment was related to ER protein processing. Furthermore, it was suspected that there was some connection with ER stress. This study continued to explore the proteins contained in this pathway, most of which were skeletal structural proteins. However, it was found that a protein called CALU could be secreted to the extracellular, and the difference in CALU expression in NSC-S was about 90 times that of control media. Therefore, the subsequent research focused on CALU. CALU, a family of multiple EF-hand proteins, regulates calcium ion pump activity and plays an important role in calcium ion homeostasis. Studies showed that CALU could relieve the ER stress of cardiomyocytes to a certain extent and protect cardiomyocytes from apoptosis(Lee et al. 2013; Wang et al. 2017; Wang et al. 2018). In this study, the morphological observation of PC12 cells showed that CALU restored the TG-induced cell damage. Further results showed that CALU restored calcium homeostasis in the cytoplasm and reduced the expression of GRP78, PERK, and other ER stress markers. Ultimately, it attenuated ER stress-induced apoptosis and rescued neurons. These results suggest that NSC-S exerts protective effects that may be associated with CALU.

Based on the fact that the TG target action is the calcium pump (SERCA) on the endoplasmic reticulum membrane, it is conjectured that CALU may exert a protective effect by restoring the activity of SERCA. The current work indicates that CALU inhibits ER stress by targeting SERCA. CALU could significantly enhance the activity of SERCA and its protein expression. Strangely, the mRNA level expression of SERCA was opposite to the protein level. This opposite result was observed after a time interval of TG injuries such as 6 h, 12 h, and 24 h with the addition of CALU recombinant protein. It is speculated whether the SERCA gene is translated into a protein and then degraded. Ubiquitination and proteasome pathways are the protein degradation pathways(Fabre et al. 2019). It has been shown that TG allows the ubiquitination of proteins(Dibdiakova et al. 2019). As shown in the results, the level of ubiquitination in TG-treated cells was significantly increased. Also, genes associated with ubiquitination such as Derlin, EDEM1, HERP1, and HRD1 were significantly up-regulated(Doroudgar et al. 2015; Kokame et al. 2000). Therefore, there is strong evidence that TG can cause ubiquitination of cells.

The addition of MG132, a specific inhibitor of ubiquitination(Seo et al. 2003), revealed a partial increase in the expression of SERCA protein. Measurement of total intracellular ubiquitination levels revealed that CALU reduced the TG-induced increase in ubiquitination levels, which were inhibited by the ubiquitination inhibitor MG132. Protein interaction map analysis showed that CALU was closely associated with

ubiquitination-related genes such as Derlin, EDEM1, HERP1, and HRD1 and that CALU also restored the expression of ubiquitination-related genes after TG induction.

Until now, current experiments can only demonstrate that CALU can reduce TG-induced cellular ubiquitination, but whether it is specific to SERCA ubiquitination and the specific form of ubiquitination needs more investigation by further experiments.

Conclusion

The study showed that NSC-S improved the prognosis of TBI by relieving TBI-induced ER stress and blocking the ER stress classical pathway-PERK-eIF2 pathway. NSC-S exerted protective effects through the PERK-eIF2 pathway. The protective roles of NSC-S may be related to CALU in the NSC-S. NSC-S is considered a promising therapeutic strategy for the treatment of TBI.

Abbreviations

NSC-S	Neural stem cell secretome
ER Stress	Endoplasmic reticulum stress
TBI	Traumatic brain injury
ROS	Reactive oxygen species
TG	Thapsigargin
PERK	RNA-dependent protein kinase
eIF2	Eukaryotic initiation factor 2
ATF4	Activating transcription factor 4
CHOP	C/EBP homologous protein

Declarations

Acknowledgment We would like to thank Professor Weining Zhang and Associate Professor Jia Wang for their help in animal experiments.

Authors' contributions Y.T.L.; Conceptualization, Methodology, Data Collection, Resources, Writing-Original Draft. M.R.; Conceptualization, Data Analysis, Supervision, Writing-Original, Review, and Editing. X.R.L.; Software, Methodology. D.D.N.; Y.Z.; Y.Q.; Y.S.; T.G.; Y.Y.N.; J.W.Z.; Z.Y.W.; Writing-Review and Editing. J.B.H.; Conceptualization, Methodology, Resources, Funding acquisition, Supervision, Writing-Review, and Editing. All authors read and approved the final manuscript.

Founding This study was supported by the National Natural Science Foundation of China (Grant No. 81571221), the Science and Technology Cooperation Foundation of Health Biomed (Grant No. 20200605) and the Qing Lan Project of Jiangsu Province, the ICTS "NANBIOSIS", in particular by the Drug Formulation Unit (U10) of the CIBER in Bioengineering, Biomaterials, and Nanomedicine (CIBER-BBN) at the University of the Basque Country (UPV/EHU) in Vitoria-Gasteiz, and the National Research Foundation of Korea (2018K1A4A3A01064257, 2021R1A5A2022318).

Data Availability Statement The data are contained within the article.

Conflicts of Interest The authors declare no conflicts of interest.

Ethical Approval All animal experiments were approved by the institutional animal care and use committee of Jiangsu University (Permit Number: SCXK 2018-0012).

References

1. Abdullahi A, Stanojcic M, Parousis A, Patsouris D, Jeschke MG (2017) Modeling Acute ER Stress in Vivo and in Vitro. Shock 47 (4):506-513. doi:10.1097/SHK.0000000000000759
2. Begum G, Yan HQ, Li L, Singh A, Dixon CE, Sun D (2014) Docosahexaenoic acid reduces ER stress and abnormal protein accumulation and improves neuronal function following traumatic brain injury. J Neurosci 34 (10):3743-3755. doi:10.1523/JNEUROSCI.2872-13.2014
3. Bertolotti A, Zhang Y, Hendershot LM, Harding HP, Ron D (2000) Dynamic interaction of BiP and ER stress transducers in the unfolded-protein response. Nature Cell Biology 2 (6):326-332. doi:10.1038/35014014
4. Borhani-Haghighi M, Mohamadi Y (2021) The protective effects of neural stem cells and neural stem cells-conditioned medium against inflammation-induced prenatal brain injury. J Neuroimmunol 360:577707. doi:10.1016/j.jneuroim.2021.577707
5. Capizzi A, Woo J, Verduzco-Gutierrez M (2020) Traumatic Brain Injury: An Overview of Epidemiology, Pathophysiology, and Medical Management. Med Clin North Am 104 (2):213-238. doi:10.1016/j.mcna.2019.11.001
6. Chang R, Zhou R, Qi X, Wang J, Wu F, Yang W, Zhang W, Sun T, Li Y, Yu J (2016) Protective effects of aloin on oxygen and glucose deprivation-induced injury in PC12 cells. Brain Res Bull 121:75-83. doi:10.1016/j.brainresbull.2016.01.001
7. Chen T, Li Y, Ni W, Tang B, Wei Y, Li J, Yu J, Zhang L, Gao J, Zhou J, Zhang W, Xu H, Hu J (2020a) Human Neural Stem Cell-Conditioned Medium Inhibits Inflammation in Macrophages Via Sirt-1 Signaling Pathway In Vitro and Promotes Sciatic Nerve Injury Recovery in Rats. Stem Cells Dev 29 (16):1084-1095. doi:10.1089/scd.2020.0020

8. Chen T, Zhu J, Wang YH, Hang CH (2020b) Arc silence aggravates traumatic neuronal injury via mGluR1-mediated ER stress and necroptosis. Cell Death Dis 11 (1):4. doi:10.1038/s41419-019-2198-5
9. Chen X, Chen C, Fan S, Wu S, Yang F, Fang Z, Fu H, Li Y (2018) Omega-3 polyunsaturated fatty acid attenuates the inflammatory response by modulating microglia polarization through SIRT1-mediated deacetylation of the HMGB1/NF-kappaB pathway following experimental traumatic brain injury. J Neuroinflammation 15 (1):116. doi:10.1186/s12974-018-1151-3
10. Chen X, Ye K, Yu J, Gao J, Zhang L, Ji X, Chen T, Wang H, Dai Y, Tang B, Xu H, Sun X, Hu J (2020c) Regeneration of sciatic nerves by transplanted microvesicles of human neural stem cells derived from embryonic stem cells. Cell Tissue Bank 21 (2):233-248. doi:10.1007/s10561-020-09816-5
11. Daneshmandi L, Shah S, Jafari T, Bhattacharjee M, Momah D, Saveh-Shemshaki N, Lo KW, Laurencin CT (2020) Emergence of the Stem Cell Secretome in Regenerative Engineering. Trends Biotechnol 38 (12):1373-1384. doi:10.1016/j.tibtech.2020.04.013
12. Deng C, Yi R, Fei M, Li T, Han Y, Wang H (2021) Naringenin attenuates endoplasmic reticulum stress, reduces apoptosis, and improves functional recovery in experimental traumatic brain injury. Brain Res 1769:147591. doi:10.1016/j.brainres.2021.147591
13. Dibdiakova K, Saksonova S, Pilchova I, Klacanova K, Tatarkova Z, Racay P (2019) Both thapsigargin- and tunicamycin-induced endoplasmic reticulum stress increases expression of Hrd1 in IRE1-dependent fashion. Neurol Res 41 (2):177-188. doi:10.1080/01616412.2018.1547856
14. Doroudgar S, Volkers M, Thuerauf DJ, Khan M, Mohsin S, Respress JL, Wang W, Gude N, Muller OJ, Wehrens XH, Sussman MA, Glembotski CC (2015) Hrd1 and ER-Associated Protein Degradation, ERAD, are Critical Elements of the Adaptive ER Stress Response in Cardiac Myocytes. Circ Res 117 (6):536-546. doi:10.1161/CIRCRESAHA.115.306993
15. Fabre B, Livneh I, Ziv T, Ciechanover A (2019) Identification of proteins regulated by the proteasome following induction of endoplasmic reticulum stress. Biochem Biophys Res Commun 517 (2):188-192. doi:10.1016/j.bbrc.2019.07.040
16. Gao C, Chen X, Xu H, Guo H, Zheng L, Yan Y, Ren Z, Luo C, Gao Y, Wang Z, Tao L, Wang T (2022) Restraint Stress Delays the Recovery of Neurological Impairments and Exacerbates Brain Damages through Activating Endoplasmic Reticulum Stress-mediated Neurodegeneration/Autophagy/Apopotosis post Moderate Traumatic Brain Injury. Mol Neurobiol 59 (3):1560-1576. doi:10.1007/s12035-022-02735-4
17. Huang C, Gan D, Fan C, Wen C, Li A, Li Q, Zhao J, Wang Z, Zhu L, Lu D (2018) The Secretion from Neural Stem Cells Pretreated with Lycopene Protects against tert-Butyl Hydroperoxide-Induced Neuron Oxidative Damage. Oxid Med Cell Longev 2018:5490218. doi:10.1155/2018/5490218
18. Hwang I, Park JH, Park HS, Choi KA, Seol KC, Oh SI, Kang S, Hong S (2013) Neural stem cells inhibit melanin production by activation of Wnt inhibitors. J Dermatol Sci 72 (3):274-283. doi:10.1016/j.jdermsci.2013.08.006

19. Jamjoom AAB, Rhodes J, Andrews PJD, Grant SGN (2021) The synapse in traumatic brain injury. Brain 144 (1):18-31. doi:10.1093/brain/awaa321
20. Jia G, Diao Z, Liu Y, Sun C, Wang C (2021) Neural stem cell-conditioned medium ameliorates Abeta25-35-induced damage in SH-SY5Y cells by protecting mitochondrial function. Bosn J Basic Med Sci 21 (2):179-186. doi:10.17305/bjbms.2020.4570
21. Kaufman RJ (2002) Orchestrating the unfolded protein response in health and disease. Journal of Clinical Investigation 110 (10):1389-1398. doi:10.1172/jci200216886
22. Khellaf A, Khan DZ, Helmy A (2019) Recent advances in traumatic brain injury. J Neurol 266 (11):2878-2889. doi:10.1007/s00415-019-09541-4
23. Kim I, Xu W, Reed JC (2008) Cell death and endoplasmic reticulum stress: disease relevance and therapeutic opportunities. Nat Rev Drug Discov 7 (12):1013-1030. doi:10.1038/nrd2755
24. Kokame K, Agarwala KL, Kato H, Miyata T (2000) Herp, a new ubiquitin-like membrane protein induced by endoplasmic reticulum stress. J Biol Chem 275 (42):32846-32853. doi:10.1074/jbc.M002063200
25. Kumar R, Azam S, Sullivan JM, Owen C, Cavener DR, Zhang P, Ron D, Harding HP, Chen JJ, Han A, White BC, Krause GS, DeGracia DJ (2001) Brain ischemia and reperfusion activates the eukaryotic initiation factor 2alpha kinase, PERK. J Neurochem 77 (5):1418-1421. doi:10.1046/j.1471-4159.2001.00387.x
26. Larner SF, Hayes RL, Wang KK (2006) Unfolded protein response after neurotrauma. J Neurotrauma 23 (6):807-829. doi:10.1089/neu.2006.23.807
27. Lee JH, Kwon EJ, Kim DH (2013) Calumenin has a role in the alleviation of ER stress in neonatal rat cardiomyocytes. Biochem Biophys Res Commun 439 (3):327-332. doi:10.1016/j.bbrc.2013.08.087
28. Li Q, Wang P, Huang C, Chen B, Liu J, Zhao M, Zhao J (2019) N-Acetyl Serotonin Protects Neural Progenitor Cells Against Oxidative Stress-Induced Apoptosis and Improves Neurogenesis in Adult Mouse Hippocampus Following Traumatic Brain Injury. J Mol Neurosci 67 (4):574-588. doi:10.1007/s12031-019-01263-6
29. Lima NCR, Melo TQ, Sakugawa AYS, Melo KP, Ferrari MFR (2019) Restoration of Rab1 Levels Prevents Endoplasmic Reticulum Stress in Hippocampal Cells during Protein Aggregation Triggered by Rotenone. Neuroscience 419:5-13. doi:10.1016/j.neuroscience.2019.08.050
30. Liu S, Lyeth BG, Hamm RJ (1994) Protective effect of galanin on behavioral deficits in experimental traumatic brain injury. J Neurotrauma 11 (1):73-82. doi:10.1089/neu.1994.11.73
31. Loane DJ, Faden AI (2010) Neuroprotection for traumatic brain injury: translational challenges and emerging therapeutic strategies. Trends Pharmacol Sci 31 (12):596-604. doi:10.1016/j.tips.2010.09.005
32. Lu P, Jones LL, Snyder EY, Tuszynski MH (2003) Neural stem cells constitutively secrete neurotrophic factors and promote extensive host axonal growth after spinal cord injury. Experimental Neurology 181 (2):115-129. doi:10.1016/s0014-4886(03)00037-2

33. Lucke-Wold BP, Logsdon AF, Turner RC, Huber JD, Rosen CL (2017) Endoplasmic Reticulum Stress Modulation as a Target for Ameliorating Effects of Blast Induced Traumatic Brain Injury. J Neurotrauma 34 (S1):S62-S70. doi:10.1089/neu.2016.4680
34. Mao L, Sun L, Sun J, Sun B, Gao Y, Shi H (2021) Ethyl pyruvate improves white matter remodeling in rats after traumatic brain injury. CNS Neurosci Ther 27 (1):113-122. doi:10.1111/cns.13534
35. Moritz KE, Geeck K, Underly RG, Searles M, Smith JS (2014) Post-operative environmental enrichment improves spatial and motor deficits but may not ameliorate anxiety- or depression-like symptoms in rats following traumatic brain injury. Restor Neurol Neurosci 32 (5):701-716. doi:10.3233/RNN-140414
36. Nakka VP, Prakash-Babu P, Vemuganti R (2016) Crosstalk Between Endoplasmic Reticulum Stress, Oxidative Stress, and Autophagy: Potential Therapeutic Targets for Acute CNS Injuries. Mol Neurobiol 53 (1):532-544. doi:10.1007/s12035-014-9029-6
37. Ni W, Zhou J, Ling Y, Lu X, Niu D, Zeng Y, Qiu Y, Si Y, Wang J, Zhang W, Wang Z, Hu J (2022) Neural stem cell secretome exerts a protective effect on damaged neuron mitochondria in Parkinson's disease model. Brain Res 1790:147978. doi:10.1016/j.brainres.2022.147978
38. Pang AL, Xiong LL, Xia QJ, Liu F, Wang YC, Liu F, Zhang P, Meng BL, Tan S, Wang TH (2017) Neural Stem Cell Transplantation Is Associated with Inhibition of Apoptosis, Bcl-xL Upregulation, and Recovery of Neurological Function in a Rat Model of Traumatic Brain Injury. Cell Transplant 26 (7):1262-1275. doi:10.1177/0963689717715168
39. Prins M, Greco T, Alexander D, Giza CC (2013) The pathophysiology of traumatic brain injury at a glance. Dis Model Mech 6 (6):1307-1315. doi:10.1242/dmm.011585
40. Ramalingam M, Jang S, Jeong HS (2021) Neural-Induced Human Adipose Tissue-Derived Stem Cells Conditioned Medium Ameliorates Rotenone-Induced Toxicity in SH-SY5Y Cells. Int J Mol Sci 22 (5). doi:10.3390/ijms22052322
41. Ratajczak MZ, Kucia M, Jadczyk T, Greco NJ, Wojakowski W, Tendera M, Ratajczak J (2012) Pivotal role of paracrine effects in stem cell therapies in regenerative medicine: can we translate stem cell-secreted paracrine factors and microvesicles into better therapeutic strategies? Leukemia 26 (6):1166-1173. doi:10.1038/leu.2011.389
42. Salikhova D, Bukharova T, Cherkashova E, Namestnikova D, Leonov G, Nikitina M, Gubskiy I, Akopyan G, Elchaninov A, Midiber K, Bulatenco N, Mokrousova V, Makarov A, Yarygin K, Chekhonin V, Mikhaleva L, Fatkhudinov T, Goldshtein D (2021) Therapeutic Effects of hiPSC-Derived Glial and Neuronal Progenitor Cells-Conditioned Medium in Experimental Ischemic Stroke in Rats. Int J Mol Sci 22 (9). doi:10.3390/ijms22094694
43. Seo HS, Yang JY, Ishikawa M, Bolle C, Ballesteros ML, Chua NH (2003) LAF1 ubiquitination by COP1 controls photomorphogenesis and is stimulated by SPA1. Nature 423 (6943):995-999. doi:10.1038/nature01696
44. Sun D, Wang J, Liu X, Fan Y, Yang M, Zhang J (2020) Dexmedetomidine attenuates endoplasmic reticulum stress-induced apoptosis and improves neuronal function after traumatic brain injury in

mice. Brain Res 1732:146682. doi:10.1016/j.brainres.2020.146682

45. Sun G, Zhao Z, Lang J, Sun B, Zhao Q (2021) Nrf2 loss of function exacerbates endoplasmic reticulum stress-induced apoptosis in TBI mice. Neurosci Lett 770:136400. doi:10.1016/j.neulet.2021.136400
46. Tang B, Ni W, Zhou J, Ling Y, Niu D, Lu X, Chen T, Ramalingam M, Hu J (2021) Peroxiredoxin 6 secreted by Schwann-like cells protects neuron against ischemic stroke in rats via PTEN/PI3K/AKT pathway. Tissue Cell 73:101635. doi:10.1016/j.tice.2021.101635
47. Tsai MJ, Tsai SK, Hu BR, Liou DY, Huang SL, Huang MC, Huang WC, Cheng H, Huang SS (2014) Recovery of neurological function of ischemic stroke by application of conditioned medium of bone marrow mesenchymal stem cells derived from normal and cerebral ischemia rats. J Biomed Sci 21:5. doi:10.1186/1423-0127-21-5
48. Verfaillie T, Rubio N, Garg AD, Bultynck G, Rizzuto R, Decuypere JP, Piette J, Linehan C, Gupta S, Samali A, Agostinis P (2012) PERK is required at the ER-mitochondrial contact sites to convey apoptosis after ROS-based ER stress. Cell Death Differ 19 (11):1880-1891. doi:10.1038/cdd.2012.74
49. Wan YJ, Wang YH, Guo Q, Jiang Y, Tu PF, Zeng KW (2021) Protocatechualdehyde protects oxygen-glucose deprivation/reoxygenation-induced myocardial injury via inhibiting PERK/ATF6alpha/IRE1alpha pathway. Eur J Pharmacol 891:173723. doi:10.1016/j.ejphar.2020.173723
50. Wang K, Wang T, Xu H, Zhong X, Huang Z (2021) Harpagide exerts a neuroprotective effect by inhibiting endoplasmic reticulum stress via SERCA following oxygen-glucose deprivation/reoxygenation injury. Neurosci Lett 753:135874. doi:10.1016/j.neulet.2021.135874
51. Wang Y, Cui X, Wang Y, Fu Y, Guo X, Long J, Wei C, Zhao M (2018) Protective effect of miR378* on doxorubicin-induced cardiomyocyte injury via calumenin. J Cell Physiol 233 (10):6344-6351. doi:10.1002/jcp.26615
52. Wang Y, Xuan L, Cui X, Wang Y, Chen S, Wei C, Zhao M (2017) Ibutilide treatment protects against ER stress induced apoptosis by regulating calumenin expression in tunicamycin treated cardiomyocytes. PLoS One 12 (4):e0173469. doi:10.1371/journal.pone.0173469
53. Wang ZF, Gao C, Chen W, Gao Y, Wang HC, Meng Y, Luo CL, Zhang MY, Chen G, Chen XP, Wang T, Tao LY (2019) Salubrinal offers neuroprotection through suppressing endoplasmic reticulum stress, autophagy and apoptosis in a mouse traumatic brain injury model. Neurobiol Learn Mem 161:12-25. doi:10.1016/j.nlm.2019.03.002
54. Wu C, Du M, Yu R, Cheng Y, Wu B, Fu J, Tan W, Zhou Q, Balawi E, Liao ZB (2022) A novel mechanism linking ferroptosis and endoplasmic reticulum stress via the circPtpn14/miR-351-5p/5-LOX signaling in melatonin-mediated treatment of traumatic brain injury. Free Radic Biol Med 178:271-294. doi:10.1016/j.freeradbiomed.2021.12.007
55. Wu F, Xu K, Liu L, Zhang K, Xia L, Zhang M, Teng C, Tong H, He Y, Xue Y, Zhang H, Chen D, Hu A (2019) Vitamin B12 Enhances Nerve Repair and Improves Functional Recovery After Traumatic Brain

Injury by Inhibiting ER Stress-Induced Neuron Injury. Front Pharmacol 10:406. doi:10.3389/fphar.2019.00406

56. Wu X, Wang C, Wang J, Zhu M, Yao Y, Liu J (2021) Hypoxia preconditioning protects neuronal cells against traumatic brain injury through stimulation of glucose transport mediated by HIF-1alpha/GLUTs signaling pathway in rat. Neurosurg Rev 44 (1):411-422. doi:10.1007/s10143-019-01228-8
57. Xing X, Huang L, Lv Y, Liu X, Su R, Li X, Dong L (2019) DL-3-n-butylphthalide Protected Retinal Muller Cells Dysfunction from Oxidative Stress. Curr Eye Res 44 (10):1112-1120. doi:10.1080/02713683.2019.1624777
58. Xiong J, Gao Y, Li X, Li K, Li Q, Shen J, Han Z, Zhang J (2020) Losartan Treatment Could Improve the Outcome of TBI Mice. Front Neurol 11:992. doi:10.3389/fneur.2020.00992
59. Xiong Y, Zhang Y, Mahmood A, Chopp M (2015) Investigational agents for treatment of traumatic brain injury. Expert Opin Investig Drugs 24 (6):743-760. doi:10.1517/13543784.2015.1021919
60. Xu G, Guo J, Sun C (2021) Eucalyptol ameliorates early brain injury after subarachnoid haemorrhage via antioxidant and anti-inflammatory effects in a rat model. Pharm Biol 59 (1):114-120. doi:10.1080/13880209.2021.1876101
61. Yang H, Wang C, Chen H, Li L, Ma S, Wang H, Fu Y, Qu T (2018) Neural Stem Cell-Conditioned Medium Ameliorated Cerebral Ischemia-Reperfusion Injury in Rats. Stem Cells Int 2018:4659159. doi:10.1155/2018/4659159
62. Yu SP, Wei Z, Wei L (2013) Preconditioning strategy in stem cell transplantation therapy. Transl Stroke Res 4 (1):76-88. doi:10.1007/s12975-012-0251-0
63. Zhou J, Ni W, Ling Y, Lv X, Niu D, Zeng Y, Qiu Y, Si Y, Wang Z, Hu J (2022) Human Neural Stem Cell Secretome Inhibits Lipopolysaccharide-Induced Neuroinflammation Through Modulating Microglia Polarization by Activating Peroxisome Proliferator-Activated Receptor Gamma. Stem Cells Dev 31 (13-14):369-382. doi:10.1089/scd.2022.0081
64. Zibara K, Ballout N, Mondello S, Karnib N, Ramadan N, Omais S, Nabbouh A, Caliz D, Clavijo A, Hu Z, Ghanem N, Gajavelli S, Kobeissy F (2019) Combination of drug and stem cells neurotherapy: Potential interventions in neurotrauma and traumatic brain injury. Neuropharmacology 145 (Pt B):177-198. doi:10.1016/j.neuropharm.2018.09.032

Figures

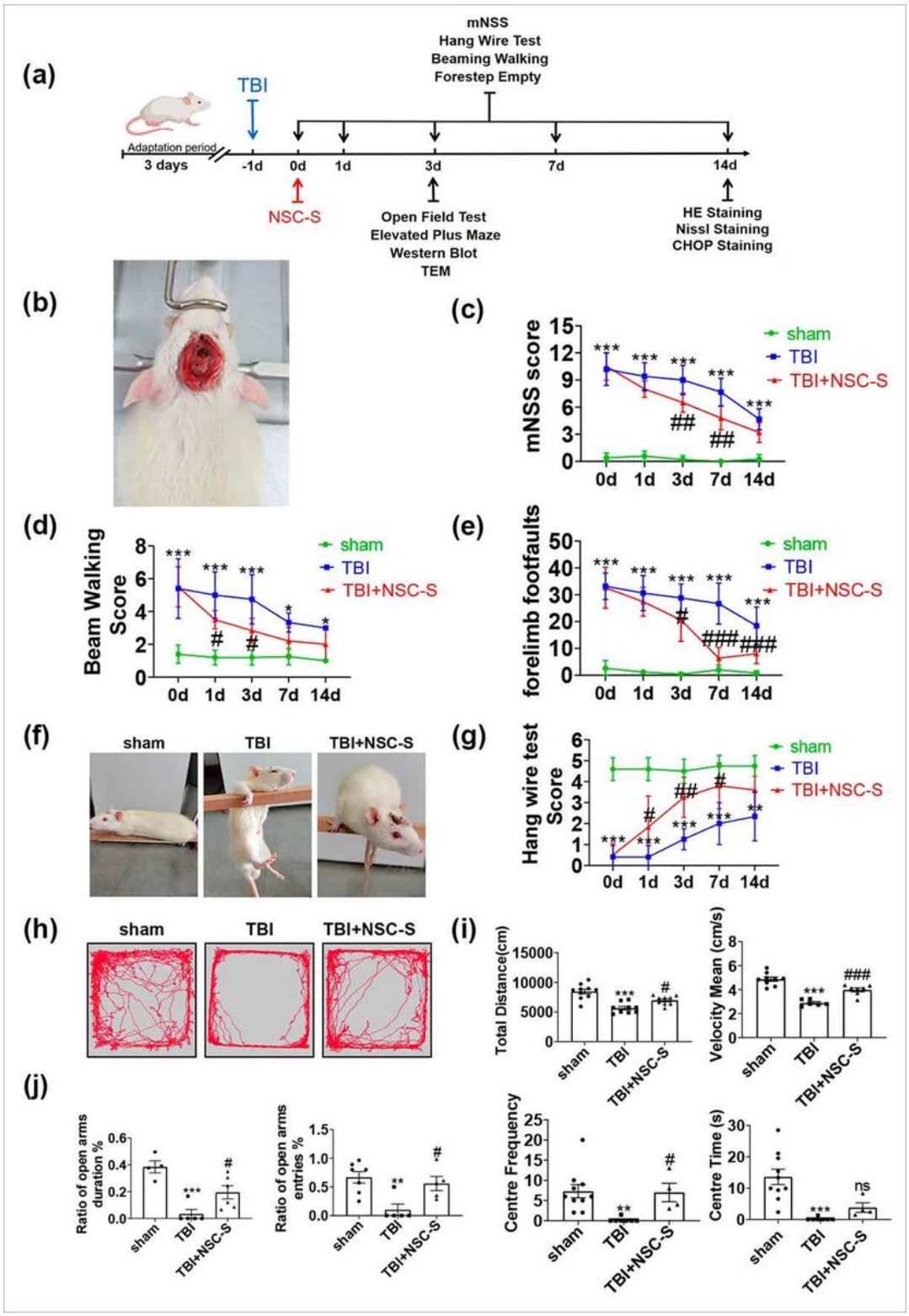

Figure 1

NSC-S improves behavior disorders in the TBI rat model

(a) Experimental timeline of brain stereotactic injection NSC-S in the treatment of TBI rat model; (b) TBI in SD rats was induced using the Feeney model; (c) mNSS neurofunction score to assess the performance of rats at days 0, 1, 3, 7 and 14 after modeling; (d) Beam walking test to evaluate the performance of rats

on days 1, 3, 7 and 14 after modeling; (e) Grid stepping test to evaluate the performance of rats on days 1, 3, 7 and 14 after modeling; (f) Hang wire test to evaluate the performance of rats on days 1, 3, 7 and 14 after modeling; (g) The scores of hang wire test; (h) Movement trajectories of rats in open field test; (i) Open field test to evaluate the total distance traveled by rats on the 3 d after modeling, the average speed of movement, the time spent in the central region, and the frequency of reaching the central region; (j) Elevated maze test to evaluate the proportion of rats reaching the open arm at 3 d after modeling, as well as the proportion of time spent in the open arm. (Data were presented as mean ± SD. n=6 per group. *P < 0.05 vs. sham group, **P < 0.01 vs. sham group, *** P < 0.001 vs. sham group; # P < 0.05 vs. TBI group, ## P < 0.01 vs. TBI group, ### P < 0.001 vs. TBI group.)

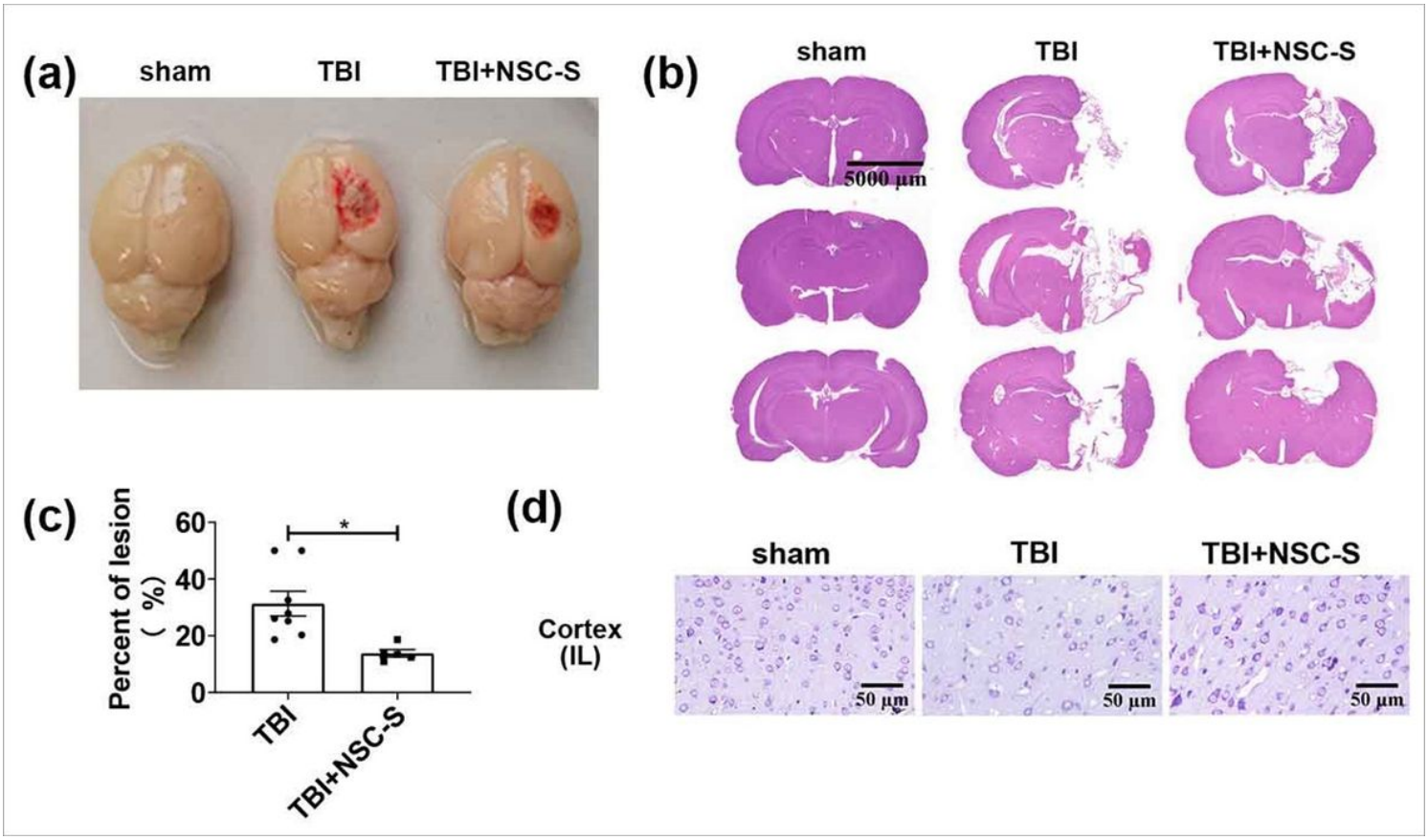

Figure 2

NSC-S relieves neuronal injury in the TBI rat model

(a) On day 14 after TBI, the physical picture of brain tissue was taken by cardiac perfusion PBS after anesthesia; (b) HE staining detected the area of brain tissue defects in rats, and each group of 3 brain tissues was from 3 different rats; (c) According to the HE results, the size of the brain tissue defect area was quantitatively described by Image J software, and the percentage of lesions = the right brain tissue defect area / the total area of brain tissue; (d) Nissl staining to observe neuronal damage in the cortical. (Data were presented as mean ± SD. n=3 per group. * P < 0.05 vs. TBI group.)

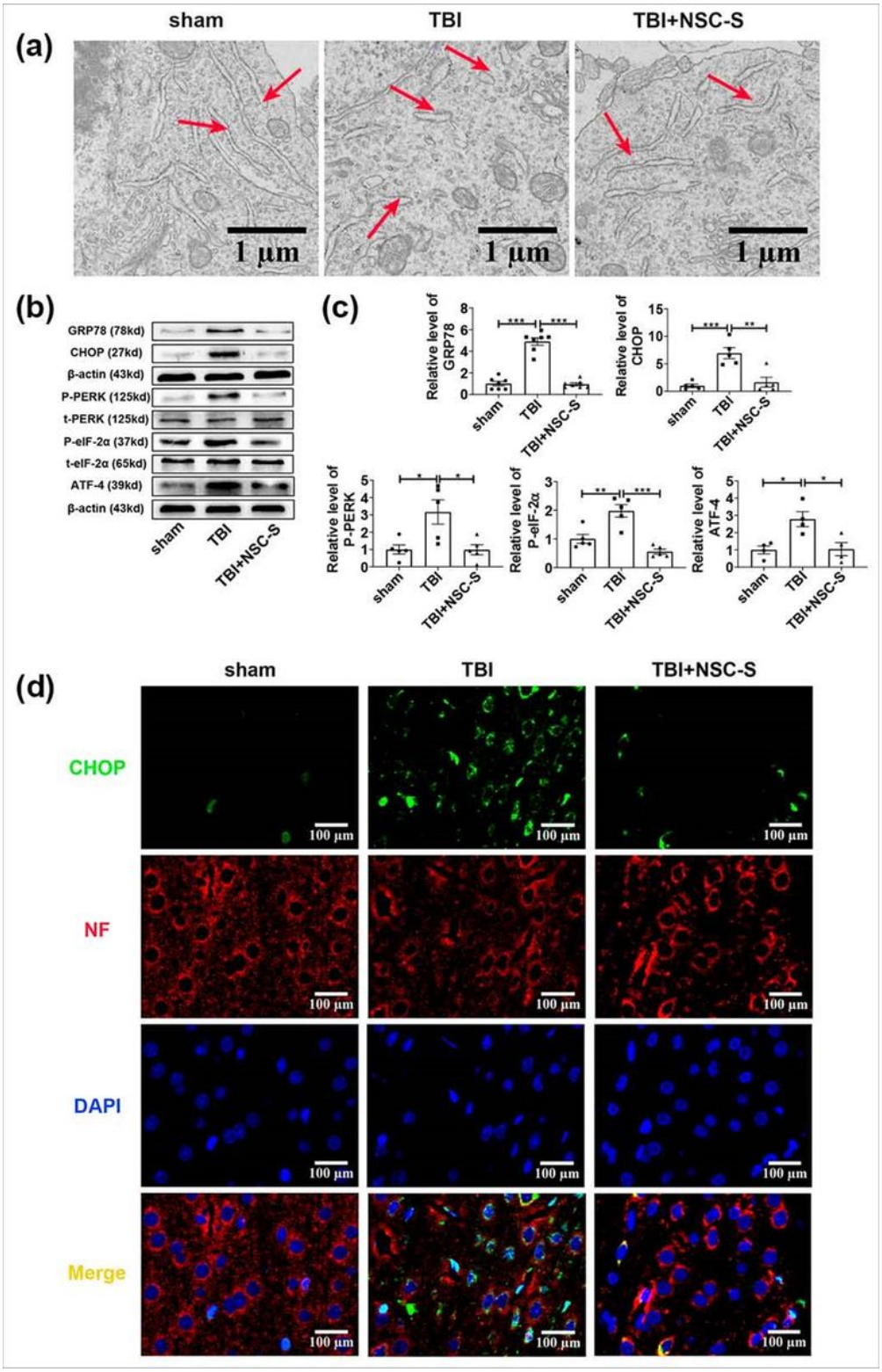

Figure 3

NSC-S restores neuronal ER stress in the TBI rat model

(a) TEM observed the morphological changes of neuronal endoplasmic reticulum in rat brain tissue, with red arrows pointing to the endoplasmic reticulum; (b) Western blot detected the levels of ER stress marker protein GRP78 and pathway-related proteins PERK, eIF-2 , ATF4, and CHOP near the ipsilateral injury area

of rat brain tissue; (c) Lane1D quantitative analysis of grayscale scanning of protein bands; (d) Immunofluorescence staining to observe CHOP expression in rat brain tissue cortex. (Data were presented as mean ± SD. n=3 per group. * $P < 0.05$, ** $P < 0.01$, *** $P < 0.001$.)

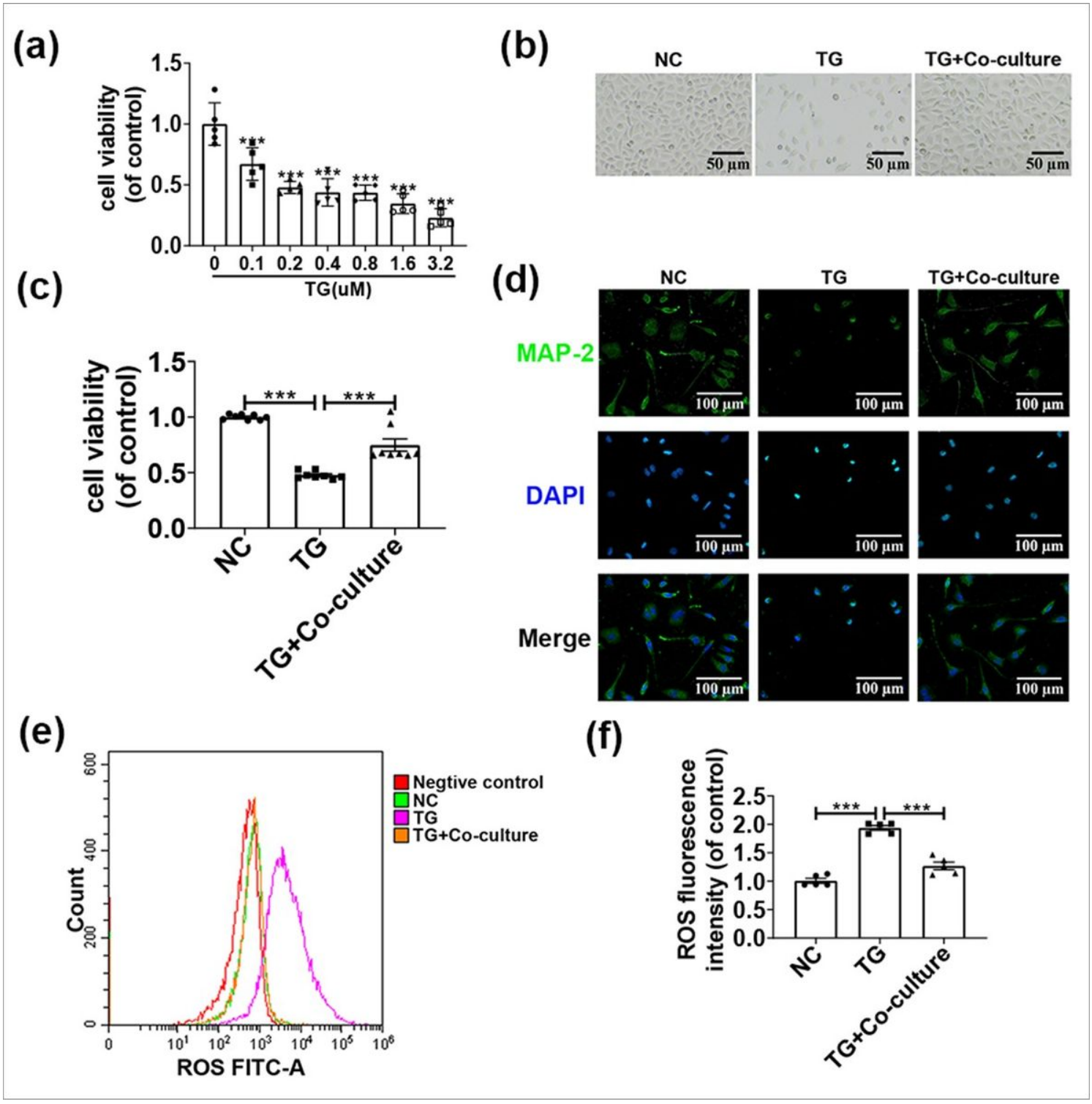

Figure 4

Co-culture with NSCs mitigates TG-induced PC12 cell damage

(a) MTT experiment to screen TG concentration; (b) Observation of morphological changes of PC12 cells in each group with ordinary light microscopy; (c) MTT experiment to detect the change of viability of PC12 cells in each group; (d) Immunofluorescence detection of MAP-2 expression in PC12 cells; (e) Flow cytometry to detect ROS levels in PC12 cells; (f) Quantitative plot of ROS level expression. (Data were presented as mean ± SD. n=3 per group. *P< 0.05, **P < 0.01, ***P < 0.001.)

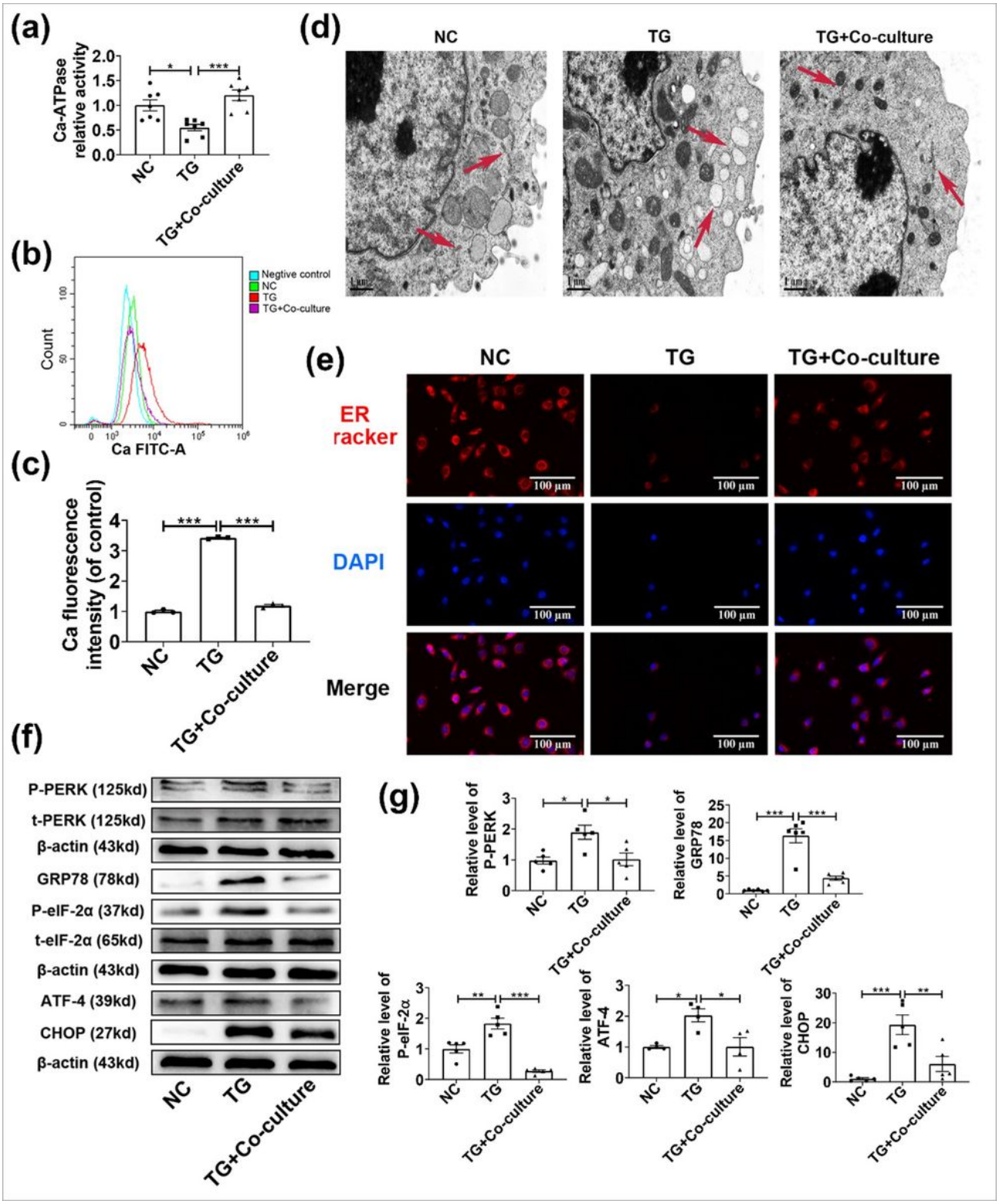

Figure 5

Co-culture with NSCs relieved TG-induced PC12 ER stress

(a) Detection of Ca^{2+}-ATPase activity in PC12 cells by full-wavelength spectrophotometer; (b) Flow cytometry to detect cytosolic Ca^{2+} levels in each group of PC12 cells; (c) Quantitative results of cytosolic Ca^{2+} levels in each group of cells; (d) TEM observed the morphological changes of endoplasmic reticulum in each group of PC12 cells, and the red arrow pointed to the endoplasmic reticulum; (e) ER Tracker probe to detect endoplasmic reticulum fluorescent probe intensity in each group of PC12 cells; (f) Western blot detected the levels of ER stress marker protein GRP78 and pathway-related proteins PERK, eIF-2 , ATF4 and CHOP in each group of PC12 cells; (g) Lane1D quantitative analysis of protein band grayscale scanning. (Data were presented as mean ± SD. n=3 per group. *P < 0.05, **P < 0.01, ***P < 0.001.)

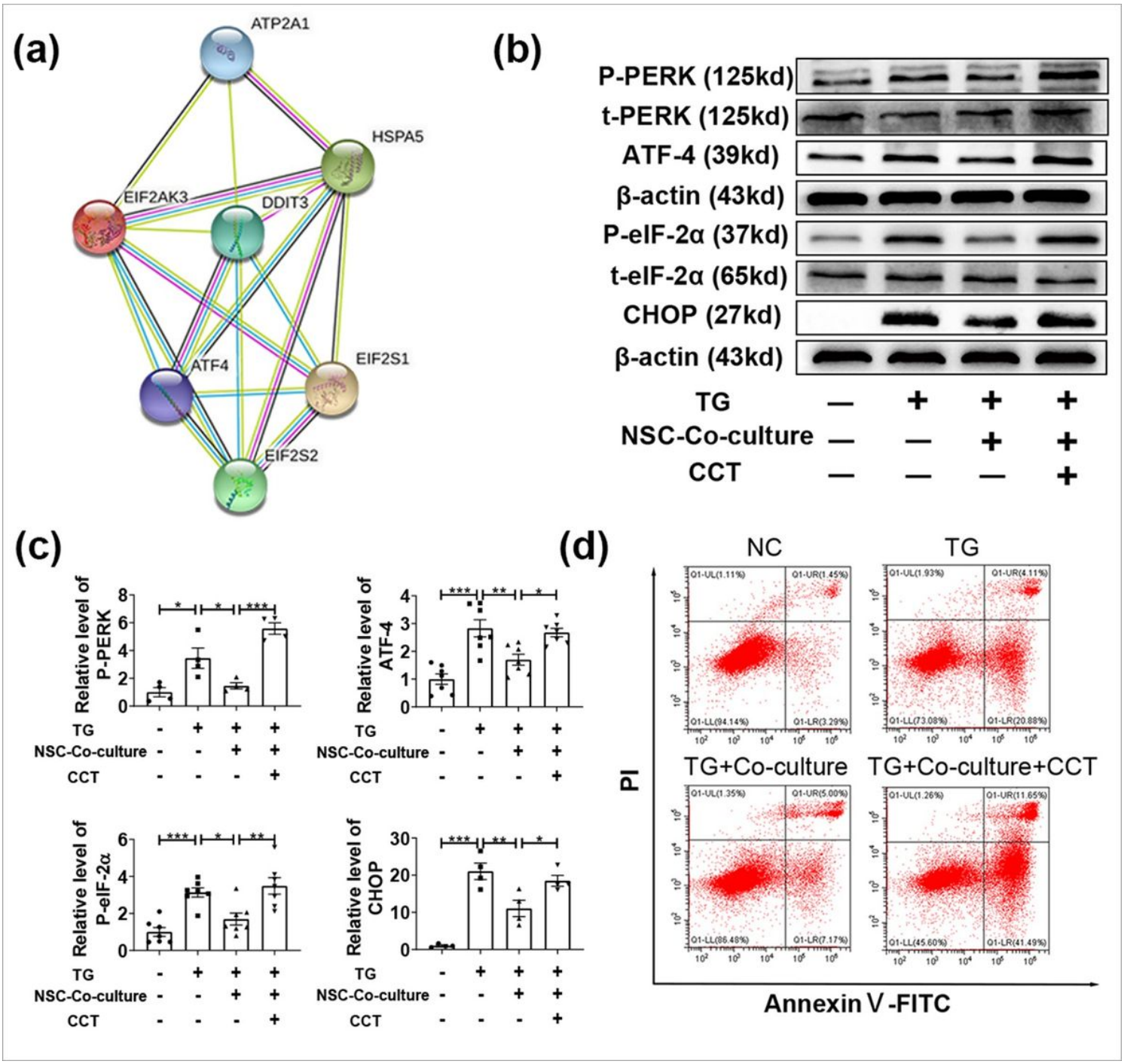

Figure 6

Co-culture with NSCs inhibits TG-induced ER stress through the PERK pathway. (a) Protein interaction diagram. Protein-protein interactions analysis through STRING resource online: https://string-db.org/. *HSPA5* means GRP78, *EIF2AK3* means PERK, *EIF2S1, EIF2S2* mean eIF-2, *DDIT3* means CHOP, *ATP2A1* means SERCA; (b) Western blot detects ER stress pathway proteins PERK, eIF-2 , ATF4, CHOP levels; (c) Lane1D quantitative analysis of grayscale scanning of protein bands; (d) Flow cytometry to detect the apoptosis level of PC12 cells in each group. (Data were presented as mean ± SD. n=3 per group. * $P < 0.05$, ** $P < 0.01$, *** $P < 0.001$.)

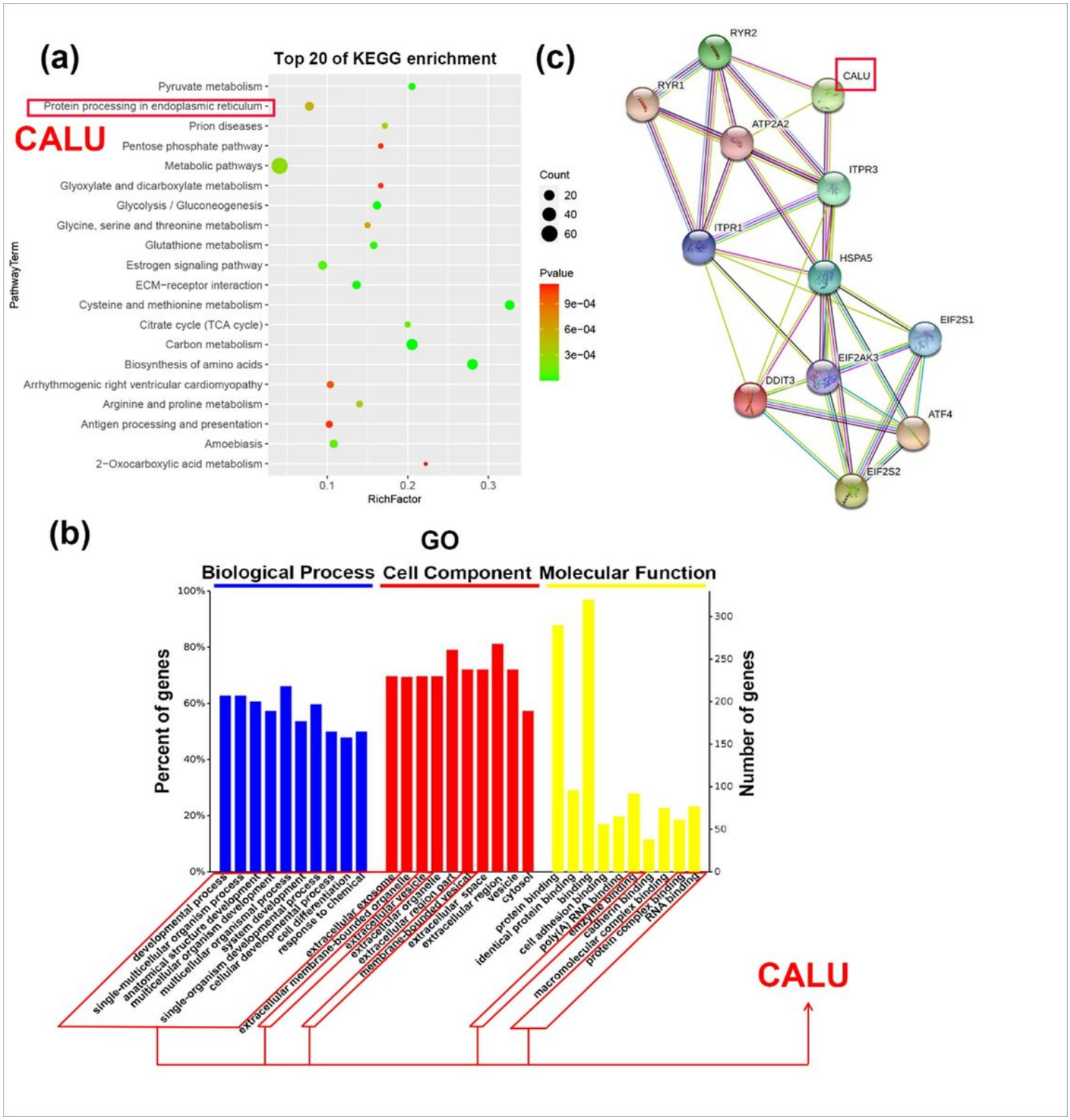

Figure 7

Bioinformatics analysis of LC-MS/MS results on NSC-S

(a) The top 20 pathways for enrichment in the KEGG analysis of NSC-S; (b) GO analysis of NSC-S enrichment in the top 10; (c) Protein interaction diagram. Protein-protein interactions analysis through STRING resource online: https://string-db.org/.

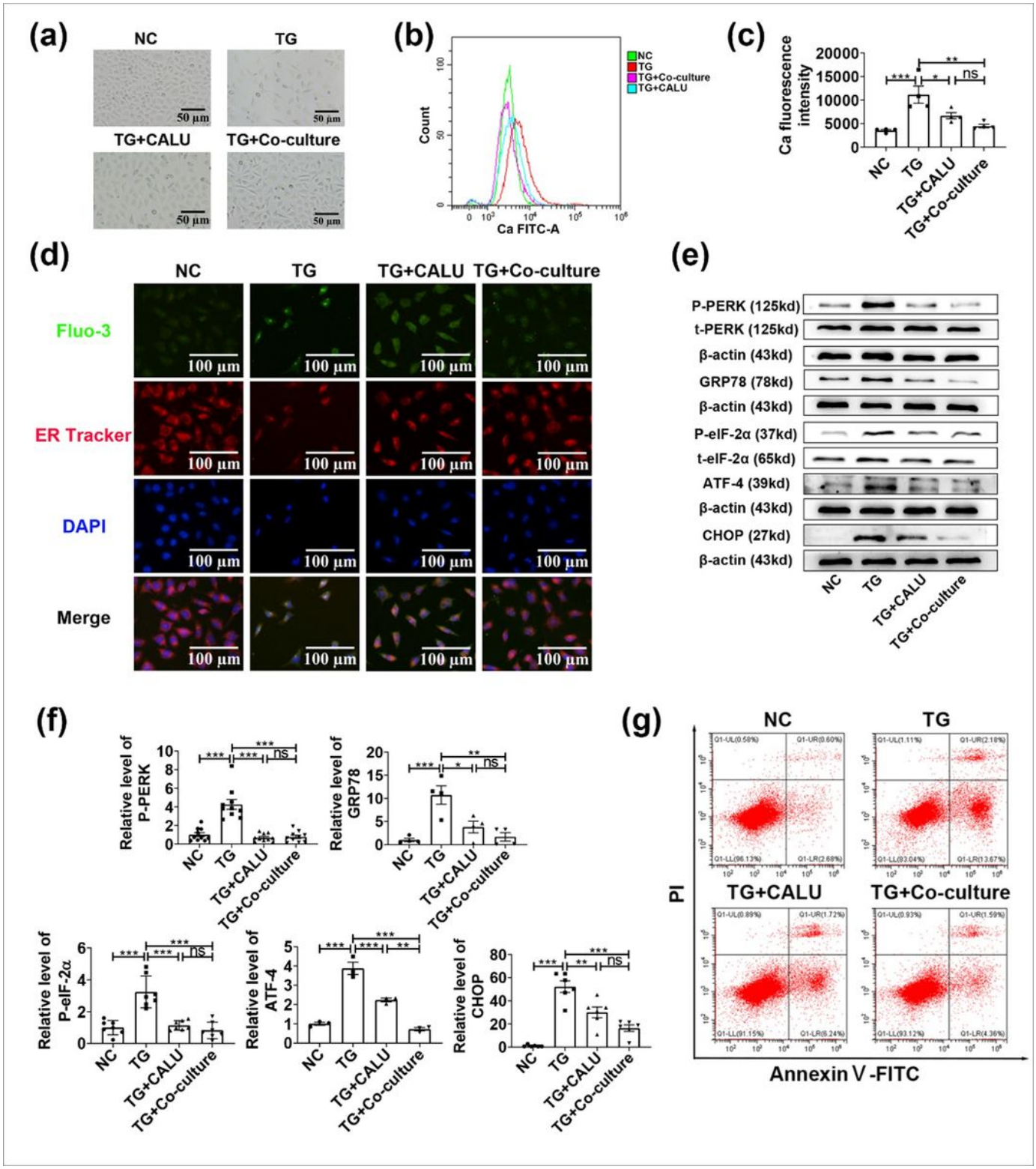

Figure 8

The CALU recombinant protein relieves ER stress in TG-induced PC12 cells through the Perk pathway

(a) Observation of morphological changes of PC12 cells in each group by general light microscopy; (b) Flow cytometry to detect cytosolic Ca^{2+} levels in each group of PC12 cells; (c) Quantitative map of cytosolic Ca^{2+} levels in PC12 cells; (d) Co-staining of cytoplasmic Ca^{2+} marker (Fluo-3) and endoplasmic

reticulum marker (ER Tracker) to detect the endoplasmic reticulum and Ca^{2+} fluorescent probe intensity of PC12 cells; (e) Western blot detected the levels of PC12 ER stress marker protein GRP78 and pathway-related proteins PERK, eIF-2 , ATF4, and CHOP; (f) Lane1D quantitative analysis of protein band grayscale scanning; (g) Flow cytometry to detect apoptosis levels of PC12 cells in each group. (Data were presented as mean ± SD. n=3 per group. *P < 0.05, **P < 0.01, ***P < 0.001.)

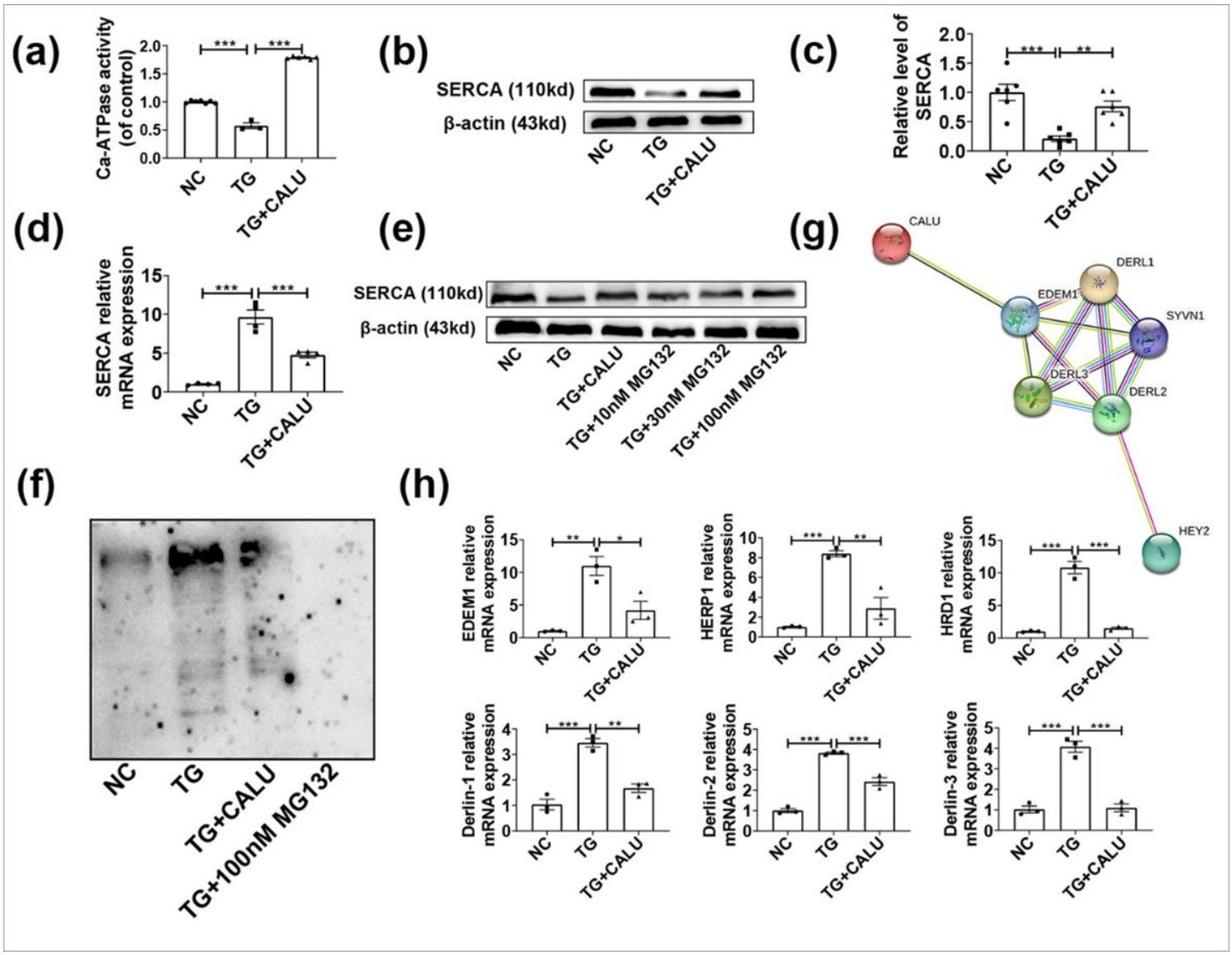

Figure 9

The CALU recombinant protein exerts protective effects by reducing cellular ubiquitination levels

(a) Detection of Ca^{2+}-ATPase activity in each group of PC12 cells by full-wavelength spectrophotometer; (b) Western blot detected the level of SERCA protein in each group of PC12 cells; (c) Lane1D quantitative analysis of grayscale scanning of protein bands; (d) qRT-PCR detected the expression of *SERCA* mRNA in each group of PC12 cells; (e) Western blot measured SERCA protein levels in PC12 cells in each group; (f) Western blot detected the ubiquitination level of PC12 cells in each group; (g) Protein interaction diagram. Protein-protein interactions analysis through STRING resource online: https://string-db.org/; (h) qRT-PCR

detected the expression of *EDEM1, HERP1, HRD1, Derlin1, Derlin2, Derlin3* mRNA in each group of PC12 cells. (Data were presented as mean ± SD. n=3 per group. **P* < 0.05, ***P* < 0.01, ****P* < 0.001.)

Supplementary Files

This is a list of supplementary files associated with this preprint. Click to download.

- floatimage1.png